THE JOURNAL OF PHYSICAL CHEMISTRY B

Article

pubs.acs.org/JPCB

Cyclodextrin-Complexation Effects on the Low-Frequency Vibrational Dynamics of Ibuprofen by Combined Inelastic Light and Neutron Scattering Experiments

Vincenza Crupi,[†] Aldo Fontana,[‡,§] Marco Giarola,[∥] Graziano Guella,[‡] Domenico Majolino,[†] Ines Mancini,[‡] Gino Mariotto,[∥] Alessandro Paciaroni,[⊥] Barbara Rossi,*[,‡,∥] and Valentina Venuti[†]

[†]Department of Physics and Earth Sciences, University of Messina, Viale Ferdinando Stagno D'Alcontres 31, 98166 Messina, Italy

[‡]Department of Physics, University of Trento, Via Sommarive 14, 38123 Povo, Trento, Italy

[§]IPCF CNR, UOS Roma, I-00185 Roma, Italy

[∥]Department of Computer Science, University of Verona, Strada le Grazie 15, 37134 Verona, Italy

[⊥]Department of Physics, University of Perugia, Via A. Pascoli, 06123 Perugia, Italy

Supporting Information

ABSTRACT: The effect of the inclusion into cyclodextrins (CD) cavity on the low-frequency vibrational dynamics of the anti-inflammatory drug ibuprofen (IBP) is here investigated by using Raman and inelastic neutron scattering (INS) experiments. The differences observed in the frequency regime 0−100 cm^{-1} between the vibrational modes of uncomplexed racemic and enantiomeric IBP are discussed on the basis of comparison with the quantum chemical computation results, taking into account the distinct symmetry properties of the molecules involved in the formation of the host−guest complex. Subsequently, the inspection of the same frequency range in the spectra of pure host methyl-β-CD and its IBP-inclusion complexes allows one to identify significant modifications in the vibrational dynamics of the guest molecule after their confinement into CD cavity. The experimental Raman and neutron spectra and the derived Raman coupling function $C^R(\omega)$ show that the complexation process gives rise to a complete amorphization of the drug, as well as to a partial hindering, in the vibrational dynamics of complexes, of the modes between 50 and 150 cm^{-1} attributed to CD molecule. The comparison between the Raman and neutron spectra of free and complexed IBP in the energy range of the Boson peak (BP) gives evidence that the dynamics related to this specific vibrational feature is sensitive to complexation phenomena.

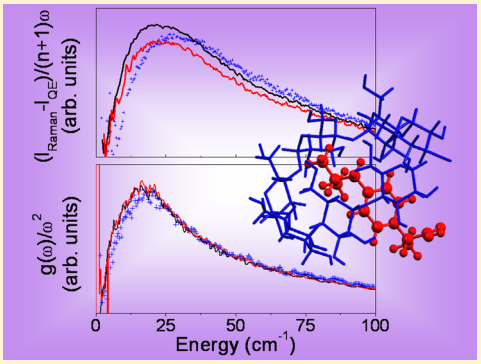

INTRODUCTION

Self-assembly phenomenon is the spontaneous organization of elementary units into more complex structures.[1] Relevant examples include molecular crystals, colloids, lipid bilayers, and phase-separated polymers[2] as well as the folding process of polypeptide chains into proteins.

The involvement of noncovalent interactions yields reversible processes and is typical of the case of molecular encapsulation or complexation, where the specific noncovalent binding of a host to a complementary guest molecule leads to the formation of host−guest (or inclusion) complexes.

The self-assembly processes are a topic of growing interest in the field of chemical physics, because many aspects concerning the mechanism of formation, stability, and network of interactions in which the components of aggregates are involved appear still not clarified. Moreover, from the applicative point of view, the above complexity permits highly innovative functionalities, and this is the reason self-assembled systems are so relevant both for material science and for pharmaceutical applications.

Cyclodextrins (CD) are natural cyclic oligosaccharides formed by 6−8 glucose units linked by 1,4-α-glycosidic bonds to form α-, β-, and γ-CD, respectively.[3−8] In water solution, they show a characteristic structure of a truncated cone in which the arrangement of the functional groups is such as to provide an internal hydrophobic (lipophilic) cavity and a slightly hydrophilic outer surface. Thanks to their properties, these molecules have the capability of including a wide range of organic compounds via noncovalent interactions,[9−11] thus altering the chemical and physical properties of the guest molecules. For this reason, considerable interest has been shown in the last years for CD, especially in the pharmaceutical field,[6−8] as demonstrated by the publication of numerous books, articles, reviews, and patents.

Moreover, various types of CD derivatives, obtained by chemical modification of the natural macrocycles, were

Received: January 16, 2013
Revised: March 19, 2013
Published: March 19, 2013

designed and proposed to increase, for example, their solubility, as in the case of methyl-β-cyclodextrin (Met-β-CD).[12]

Finally, due to the presence of asymmetric centers in their chemical structure, CD show the ability to discriminate between suitable enantiomers, forming diastereomeric complexes with slightly different stabilities.[13−18]

Ibuprofen (4-isobutyl-2-phenylpropionic acid, IBP) is an anti-inflammatory drug widely used as nonsteroidal analgesic and anti-inflammatory agent (NSAID) in many pharmaceutical preparations.[19,20] Because of the presence in its chemical structure of a stereogenic carbon, IBP can exist in two enantiomeric forms, (*R*)- and (*S*)-IBP, but only the (*S*)-isomer is capable of inhibiting cyclooxygenase (COX) at clinically relevant concentrations.

The modifications on the vibrational properties of IBP produced by its inclusion into native and modified cyclodextrins have been recently investigated, in the solid state, in the medium- and high-wavenumber ranges by using Raman scattering, Fourier transform infrared spectroscopy in the attenuated total reflectance (FTIR-ATR) configuration, and density functional theory (DFT) calculations.[21−24] From the enthalpy changes associated with the "host−guest" interactions in the solid phase, as estimated by temperature-dependent studies,[22,23] Met-β-CD turned out to be the optimal partner for IBP. In addition, a detailed analysis on the influence of chirality of IBP on its CD complexation mechanism has been carried out in solid[24,25] and liquid phases[26] by using neutron scattering, UV−vis absorption measurements, and nuclear magnetic resonance (NMR) spectroscopy. These studies revealed that the inclusion complexes formed by CD with the IBP-enantiomers are more stable with respect to the complexes of the racemate, due to a more difficult breaking of the intermolecular dimeric hydrogen bond between (*R*)- and (*S*)-IBP in the pure form.[24]

In this work, we report on the detailed analysis of the low-frequency Raman and inelastic neutron scattering (INS) spectra, in the 0−200 cm^{-1} region, of the inclusion complexes formed by Met-β-CD with the racemate (*R*,*S*)-IBP and the enantiomer (*S*)-IBP with the aim to further explore the effects on the vibrational dynamics of IBP induced by confinement into the CD cavity.

The study focuses on the inspection of the low-frequency spectral range of light and inelastic spectra, which is particularly distinctive of the amorphous and crystalline state of the matter: it is expected to give important information on the phase transformation of IBP confined in CD, through the analysis of the collective motions of the system.[27] As a matter of fact, the amorphization of drugs is one of the possible factors responsible for the enhancement of dissolution rate of active molecules, which can lead to a significant improvement of their bioavailability.[27−29]

The combined use of two different and complementary probes (light and neutrons) allows one to yield a detailed insight into the density of vibrational states of IBP-inclusion complexes, contributing to give an overall picture of the mechanism of confinement of IBP in the CD cavity.

MATERIALS AND METHODS

A. Preparation of CD Complexes. Methyl-β-cyclodextrin (Met-β-CD, degree of substitution ∼1.7−1.9) was purchased from Fluka Chemie (Switzerland). (*R*,*S*)- and (*S*)-IBP were acquired from Sigma-Aldrich. All of the reagents were used without further purification.

Before the inelastic light and neutron scattering experiments were performed, the samples of uncomplexed (*R*,*S*)-IBP and (*S*)-IBP were previously dissolved in water (the solvent where the CD complexes are then investigated) and dried in a vacuum chamber using P_2O_5 as dehydrating agent. In this way, we can avoid differences due to polymorphism and point out only the changes due to the arrangement of atoms around the stereogenic center of the molecules.

For the preparation of complexes, Met-β-CD was dissolved in water to obtain a 0.1 mM solution; subsequently, another 1 mL of water was added and the mixture was stirred at 50 °C to obtain a clear solution. An equimolar amount of dry (*R*,*S*)-IBP or (*S*)-IBP was added to this solution, and the resulting dispersion was stirred at 50 °C for 2 h to obtain a white dispersion. The liquid phase was removed to leave the inclusion complex as a white solid, which was dried in a vacuum chamber, using P_2O_5 as dehydrating agent. Electrospray ionization mass spectrometry (ESI−MS, Bruker Esquire spectrometer) measurements and NMR (Bruker Avance 400 spectrometer) analysis allowed one to establish the effective complex formation and to obtain information on its stoichiometry, which turned out to be 1:1.[21]

B. Raman Scattering Measurements. All of the Raman measurements were acquired on dried samples deposited on a glass slide, in air and at room temperature. All of the spectra were registered in backscattering geometry, in crossed polarization by using a triple-monochromator spectrometer (Horiba-Jobin Yvon, model T64000) set in double-subtractive/single configuration and equipped with 1800 grooves/mm. Micro-Raman spectra were excited by the 647.1 nm wavelength of an argon/krypton ion laser and detected by a CCD detector cryogenically cooled by liquid nitrogen. Exciting radiation was focused onto the sample surface with a spot size of about 1 μm^2 through a 80× objective with NA = 0.75. The resolution was about 0.36 cm^{-1}/pixel.

For a better comparison, all of the Raman spectra were normalized to the total area.

C. Computational Methods. The ab initio quantum chemical computations on the (*R*,*S*)-IBP and (*S*)-IBP dimers were performed with the Gaussian 03 program suite[30] using unrestricted Density Functional Theory (DFT). The nonlocal B3LYP functional hybrid method was employed, and the standard 6-311G basis set was used for the geometry optimization and vibrational energy analysis. For the plot of the theoretical Raman spectra, a Lorentzian line shape with a line width of 4 cm^{-1} was used; computed Raman activities are expressed in arbitrary units.

D. Neutron Scattering Experiments. Neutron scattering experiments were performed at Laboratoire Léon Brillouin (LLB, Saclay, France) using the time-of-flight (TOF) spectrometer MIBEMOL.[25]

Measurements were carried out at T = 300 K using neutrons with an incident wavelength of 6 Å, with a Q-independent experimental resolution of 90 μeV (defined as the full-width half-maximum of a vanadium standard). The covered Q-range was from 0.49 to 1.73 $Å^{-1}$. The explored energy range was from −45 to about 1.4 meV. In all of the figures here reported, the sign of the energy transfer has been changed for the sake of simplicity.

As sample holder, a standard, indium sealed, flat aluminum cell with variable internal spacing was used. In particular, a thickness of 0.2 mm was used for both (*R*,*S*)-IBP and (*S*)-IBP, and for their inclusion complexes with Met-β-CD, whereas a

thickness of 0.5 mm was used for Met-β-CD. For each measurement, the sample holder was placed at an angle of 135° with respect to the incident beam direction. The time of data acquisition was about 12 h. A transmission of ∼96% was obtained for IBP, of ∼91% for Met-β-CD, and of ∼94% for IBP/Met-β-CD inclusion complexes. An estimate of the multiple scattering confirms that it is below 10% on the elastic peak for all systems, thus affecting in a similar way all of the analyzed samples, so multiple scattering contributions have been neglected.

The measured time-of-flight spectra were analyzed with QENSH data treatment program, available at LLB, that allows, inter alia, the calibration of the detectors with the vanadium spectra, the correction for the empty cell, the transformation of the TOF spectra into energy spectra, and the data grouping to improve the corresponding signal/noise ratio.

E. Theoretical Background. It is well-known[31−33] that Raman spectroscopy applied to many-particle systems allows one to probe the fluctuations of the polarizability tensor due to elementary excitation, like vibrations. In the case of disordered systems, these excitation modes are expected to show a continuous frequency distribution, extending from zero to the Debye frequency of the material. In the contribution to the inelastic spectrum due to the diffusion motions (rotations and translations), these modes can be separated from the oscillatory motion if, on the time scale of typical vibrational periods, the atoms are assumed to vibrate around identifiable "quasi-equilibrium" positions. Under these approximation, the polarizability fluctuations depend linearly on the atomic displacements and the Raman spectral density will reflect the Fourier transform of the displacement−displacement correlation function, and hence the vibrational density of states (VDOS). In particular, the general approach to the description of the spectra is the disorder-induced scattering, assuming that excitations in disordered systems have no well-defined wavevector Q. So they may all contribute to the light scattering spectra.

Generally speaking, the experimental Raman intensity $I_{\mathrm{Raman}}(\omega,T)$ shows, in the low-frequency regime, two contributions:

$$I_{\mathrm{Raman}}(\omega, T) \propto I^{\mathrm{Inel}}_{\mathrm{Raman}}(\omega, T) + I_{\mathrm{QE}}(\omega) \tag{1}$$

where the inelastic intensity $I^{\mathrm{Inel}}_{\mathrm{Raman}}(\omega,T)$ is assumed to be proportional to the density of states and $I_{\mathrm{QE}}(\omega)$ is the quasi elastic scattering contribution, appearing as a broadening of the elastic line shape centered at zero frequency. $I_{\mathrm{QE}}(\omega)$ is related to diffusion motions and local reorientations, and it can be subtracted from the experimental profiles to isolate only the inelastic component of the spectra.

The inelastic Raman intensity is proportional to the density of vibrational states $g(\omega)$[34] by the relation:

$$I^{\mathrm{Inel}}_{\mathrm{Raman}}(\omega, T) \propto \frac{g^{\mathrm{R}}(\omega)[n(\omega, T) + 1]}{\omega} \tag{2}$$

where $g^{\mathrm{R}}(\omega)$ is the convolution of the $g(\omega)$ with a frequency-dependent light-to-excitation coupling factor $C^{\mathrm{R}}(\omega)$:

$$g^{\mathrm{R}}(\omega) = \int C^{\mathrm{R}}(\omega - \omega')g(\omega')\,\mathrm{d}\omega' \tag{3}$$

ω is the harmonic amplitude factor, and $n(\omega,T) = [\exp(-\hbar\omega/k_{\mathrm{B}}T) - 1]^{-1}$ is the temperature Bose factor. On the basis of the Shuker−Gammon model,[31] we can write:

$$g^{\mathrm{R}}(\omega) = C^{\mathrm{R}}(\omega)g(\omega) \tag{4}$$

The Raman coupling function $C^{\mathrm{R}}(\omega)$ is a priori unknown,[32,33] and it can be experimentally obtained by measuring $g(\omega)$ with an independent probe, for example, by means of INS measurements.[35]

The intensity measured in the neutron scattering experiment corresponds to the incoherent double-differential cross section, which is given by

$$\left(\frac{\partial^2\sigma}{\partial\Omega\partial\omega}\right)_{\mathrm{inc}} = \frac{k}{k_0}N\frac{\sigma_{\mathrm{inc}}}{4\pi}S_{\mathrm{inc}}(Q, \omega) \tag{5}$$

In the above equation, the momentum transfer is defined by $\hbar\vec{Q} = \hbar(\vec{k} - \vec{k}_0)$, $\vec{k}$ and $\vec{k}_0$ being the scattered and incident neutron wavevectors, respectively.

In the one-phonon approximation, $S_{\mathrm{inc}}(Q,\omega)$ can be written, at a given temperature T, as the sum of three components:

$$S_{\mathrm{inc}}(Q, \omega) = e^{-2W(Q,T)}\{A_0(Q)\delta(\omega) + [1 - A_0(Q)]S_{\mathrm{QE}}(Q, \omega) + S_{\mathrm{INEL}}(Q, \omega)\}R(Q, \omega) \tag{6}$$

where $S_{\mathrm{Inel}}(Q,\omega)$ is proportional to the one-phonon density of vibrational states (VDOS) $g(\omega)$ through the relation:

$$S_{\mathrm{INEL}}(Q, \omega) \propto \frac{g(\omega)[n(\omega, T) + 1]}{\omega} \tag{7}$$

Hence, from an experimental point of view, a good way to obtain the most reliable Raman coupling function $C^{\mathrm{R}}(\omega)$ is by combining eqs 2 and 7, in determining the point-by-point ratio between $I_{\mathrm{Raman}}(\omega,T)$ and $S_{\mathrm{INEL}}(Q,\omega)$.

For the comparison of light and neutron scattering data, the Raman and neutron intensities were converted into the imaginary part of the dynamical susceptibility according to the relations $\chi''_{\mathrm{R}}(\omega) = I_{\mathrm{Raman}}(\omega,T)/[n(\omega,T) + 1]$ and $\chi''_{\mathrm{N}}(\omega) = S_{\mathrm{INEL}}(Q,\omega)/[n(\omega,T) + 1]$, respectively.

Moreover, to eliminate the temperature dependence of the Raman bands, the Raman intensity was converted into the reduced Raman intensity $I_{\mathrm{red}}(\omega) = I_{\mathrm{Raman}}(\omega,T)/[n(\omega,T) + 1]\omega$, where $I^{\mathrm{red}}(\omega) \approx C^{\mathrm{R}}(\omega)g(\omega)/\omega^2$ at room temperature.

RESULTS AND DISCUSSION

A. Low-Frequency Vibrational Dynamics of (*R*,*S*)-IBP and (*S*)-IBP. In Figure 1a,b, the experimental Raman intensities of pure guest molecules (*R*,*S*)-IBP and (*S*)-IBP are reported, respectively, in the wavenumber range 0−120 cm^{-1}. Two contributions can be observed in the experimental spectra of both of the samples in this spectral region: the quasi elastic (QE) scattering, related to diffusive and relaxational dynamics of the system, that appears as a broadening of the elastic peak and the inelastic vibrational component.

Because for the purpose of this work we are only interested in the modifications occurring on the vibrational dynamics of IBP and its inclusion complexes, the Raman spectra were analyzed after subtraction of QE contribution from the total experimental profile. To evaluate the quasi elastic signal, a well-assessed fitting procedure, widely implemented for several compounds, was followed.[36−39]

The QE term turned out to be well reproduced by using a Lorentzian function, centered at zero wavenumber, having amplitude A and width Γ (dashed red line in Figure 1a,b):

dx.doi.org/10.1021/jp400509r | J. Phys. Chem. B 2013, 117, 3917−3926

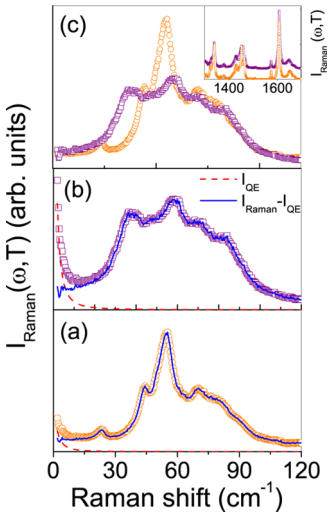

Figure 1. Experimental Raman intensity $I_{Raman}(\omega,T)$ for (*R*,*S*)-IBP (a) and (*S*)-IBP (b) together with the fit of the QE contribution (dashed red line) and after subtraction of I_{QE} (continuous blue line) in the low-wavenumber range 0−120 cm^{-1}. Comparison between Raman intensity of (*R*,*S*)-IBP (○) and (*S*)-IBP (□) after subtraction of QE contribution in the wavenumber range 0−120 cm^{-1} (c) and 1300−1700 cm^{-1} (inset). The spectra in the inset are vertically shifted for the sake of clarity.

$$I_{QE}(\omega) = \frac{A\Gamma}{\Gamma^2 + \omega^2} \quad (8)$$

By comparing the total experimental Raman intensity (empty symbols in Figure 1a,b) with the spectra obtained after subtraction of the I_{QE} (continuous blue line in the same graphs), we can observe that, for (*R*,*S*)-IBP and (*S*)-IBP, the quasi-elastic signal is negligible with respect to the inelastic scattering at wavenumber larger than ∼15 cm^{-1}. This finding was somehow expected, taking into account that IBP does not contain plasticizing water molecules, and therefore it behaves like a harmonic solid in a semicrystalline phase, according to previous quasi elastic neutron scattering (QENS) measurements performed on the same systems at T = 150 and 300 K.[25]

Focusing only on the inelastic components shown in Figure 1c, significant differences in the vibrational dynamics of (*R*,*S*)-IBP and (*S*)-IBP can be observed in the low-frequency range, while no appreciable variation appears by comparing their vibrational spectra at higher wavenumber (see inset of Figure 1c). More in detail, a larger number of low frequency modes, which are connected to large amplitude spatial motions, are observed for (*S*)-IBP with respect to (*R*,*S*)-IBP. This finding suggests the exhibition of a softer structure for the (*S*)-enantiomer with respect to racemate, probably due to the different arrangement of IBP molecules in the unit cell, which affects the vibrational density of states of the samples.

The differences observed in the experimental Raman spectra are consistent with the results of inelastic neutron scattering experiments, as pointed out in Figure 2 where the dynamic susceptibilities $\chi''(\omega)$ as obtained by the Raman (a) and INS (b) spectra for (*R*,*S*)-IBP (○) and (*S*)-IBP (□) are compared in the spectral range 0−200 cm^{-1}. The representation of the inelastic light and neutron intensities in terms of susceptibilities enhances the differences observed between the vibrational dynamics of (*R*,*S*)-IBP and (*S*)-IBP at energies lower than ∼100 cm^{-1}.

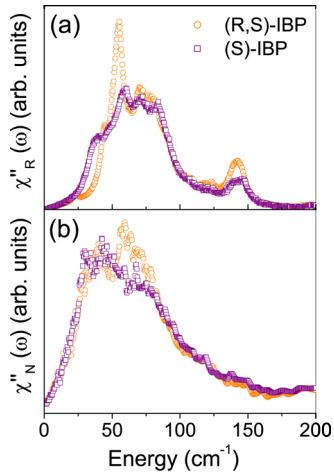

Figure 2. Dynamic susceptibility $\chi''^{R,N}(\omega)$ as obtained by the low-energy Raman (a) and INS (b) spectra for (*R*,*S*)-IBP (○) and (*S*)-IBP (□) in the spectral range 0−200 cm^{-1}.

The presence of several and partially resolved spectral components in both the low-energy Raman and the neutron spectra of (*R*,*S*)-IBP and (*S*)-IBP (Figure 2a and b) seems to suggest that the samples are in semicrystalline phase, in agreement with previous works.[40,41]

The experimentally observed differences in the low-frequency vibrational spectra can be explained by taking into account the distinct symmetry properties exhibited by the racemate and the two enantiomeric forms of IBP.[21−24] According to previous X-ray diffraction[40,41] and vibrational spectroscopy studies,[21,23] IBP prevalently develops in condensed phase dimeric entities derived from symmetric hydrogen bonding (HB) between the two carboxylic groups of adjacent molecules. As sketched by the molecular models of Figure 3a,b, the dimer of (*R*,*S*)-IBP is formed by hydrogen bonds across a center of inversion, with one molecule in the (*R*)- and the other in the (*S*)-configuration. In contrast, in the unit cell of dimeric (*S*)-IBP, the same HB constrain forces the molecules into a different 3D-arrangement.[23]

The total energies computed at the DFT level for the two different models of Figure 3a,b suggest that the energy of (*R*,*S*)-

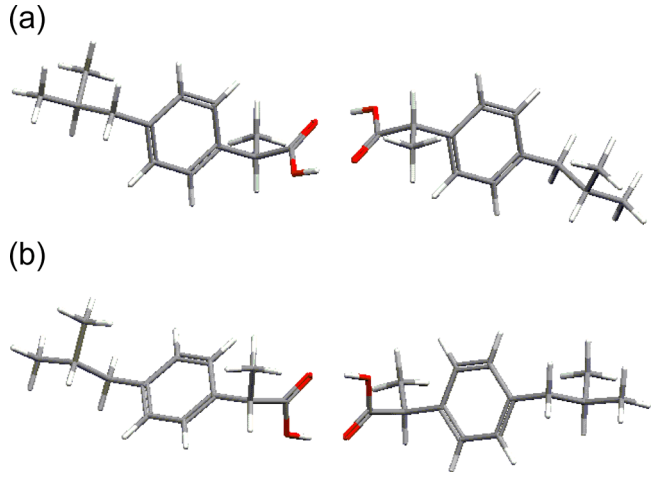

Figure 3. DFT-minimized structure for dimers of (*R*,*S*)-IBP (a) and (*S*)-IBP (b). The full list of the atom labeling is given in the Supporting Information.

dx.doi.org/10.1021/jp400509r | J. Phys. Chem. B 2013, 117, 3917−3926

IBP is lower by about 0.46 kcal/mol with respect to (*S*)-IBP dimer, which is consistent with other molecular mechanics computations.[42]

To understand the nature of the low-frequency vibrational modes, the theoretical Raman intensities was computed for dimers of (*R*,*S*)-IBP and (*S*)-IBP (Figure 4a and b,

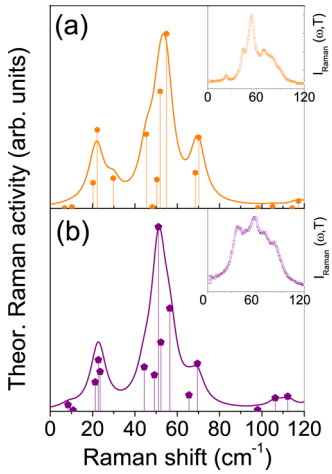

Figure 4. Theoretical Raman intensities computed for dimers of (*R*,*S*)-IBP (a) and (*S*)-IBP (b) in the wavenumber range 0−120 cm^{-1}. Inset: Experimental Raman intensities for (*R*,*S*)-IBP (○) and (S)-IBP (□).

respectively). The results are compared to the corresponding experimental spectra (insets of Figure 4) in the wavenumber range 0−120 cm^{-1}. The slight discrepancy found between the experimental and computed spectra is thought to derive from solid-state effects not taken into account by our quantum chemical computations, the noncovalent interactions among vicinal dimers arranged in the crystal lattice.

The vibrational analysis allows one to identify the type of vibrations corresponding to the computed normal modes for both of the dimeric structures of Figure 3, as summarized in Table 1.

In Figure 5 we compare the normalized displacements r_i (i = 1, 3*N*, where *N* is the number of the atoms for the structures of Figure 3, labeled as in the Supporting Information) under the effect of the normal modes at 20, 22, 30, 45, 48, 50, 52, 55, 69,

Table 1. Vibrational Analysis for Dimers of (*R*,*S*)-IBP and (*S*)-IBP[a]

	(*R*,*S*)-IBP dimer		(*S*)-IBP dimer	
normal mode number	freq/ cm^{-1}	Raman activity	freq/ cm^{-1}	Raman activity
1	20	0.7083	24	1.1348
2	22	2.1587	23	1.4704
3	30	0.8278	21	0.8353
4	45	2.0377	44	1.2646
5	48	0.0392	56	2.9468
6	50	0.7941	49	1.0400
7	52	3.2121	51	5.2750
8	55	4.7958	52	1.9714
9	69	0.9801	66	0.4620
10	70	1.9523	70	1.3661

[a]Frequencies and Raman activity computed at the DFT-B3LYP level of theory using the standard 6-311G basis set on the geometry-optimized structures of Figure 3.

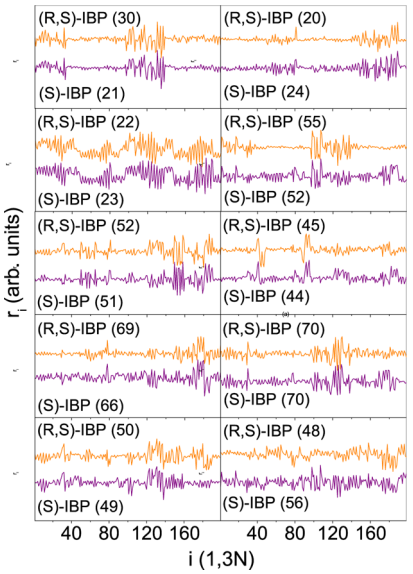

Figure 5. Normalized displacements r_i as a function of the atomic degree of freedom *i* for each atom of (*R*,*S*)-IBP (orange line) and (*S*)-IBP (purple line) under the effect of the normal modes at 20, 22, 30, 45, 48, 50, 52, 55, 69, and 70 cm^{-1} for (*R*,*S*)-IBP and 21, 23, 24, 44, 49, 51, 52, 66, and 70 cm^{-1} for (*S*)-IBP. (The full list of the atom numbers is given in the Supporting Information.)

and 70 cm^{-1} for (*R*,*S*)-IBP and 21, 23, 24, 44, 49, 51, 52, 66, and 70 cm^{-1} for (*S*)-IBP. Using this representation of the eigenvectors, we can visualize the Cartesian displacements $r_1 = X_1$, $r_2 = Y_1$, $r_3 = Z_1$, $r_4 = X_2$, etc., for each atom, due to the action of the corresponding normal mode. The comparison among the eigenvectors allows one to identify similar types of vibrations for (*R*,*S*)-IBP and (*S*)-IBP, as pointed out in Figure 5.

A difference of about 10 cm^{-1} is observed between the values of the frequencies of the computed normal mode number 3, which is found at 30 cm^{-1} for (*R*,*S*)-IBP and at 21 cm^{-1} for (*S*)-IBP dimer (see Table 1). This mode corresponds to vibrations that are mainly localized on the aryl ring and the isobutyl group of the (*R*)-enantiomer of the (*R*,*S*)-IBP dimer, while in the case of (*S*)-IBP the vibration involves the aryl ring and the isobutyl group of only one of the two (*S*)-enantiomers. Similarly, the mode number 5 is found at 48 cm^{-1} (Raman inactive mode) in the computed vibrational spectrum of (*R*,*S*)-IBP, while it is observed at 56 cm^{-1} in that of (*S*)-IBP (Raman active mode). This mode corresponds to vibrations involving the entire dimers.

B. Effect of Complexation on the Density of Vibrational States. To identify the effects of CD encapsulation on the vibrational dynamics of guest molecule IBP, in Figure 6a,b we compare the reduced Raman intensity, obtained after subtraction of the QE contribution, with the quantity $g(\omega)/\omega^2$ found by neutron data for pure Met-β-CD (blue +) and its inclusion complexes formed with (*R*,*S*)-IBP (black line) and (*S*)-IBP (red line).

At first, we can note that the vibrational spectrum of the pure host Met-β-CD (Figure 6c) appears, in the frequency range below 100 cm^{-1}, very different with respect to the profile of free (*R*,*S*)-IBP and (*S*)-IBP shown in Figure 1. For the macrocycle, in fact, in addition to the QE contribution, only a broad bump referred to as Boson peak (BP)[43−47] and centered at about 25−30 cm^{-1} can be found in the Raman spectrum at low wavenumbers (Figure 6c). The presence of the BP, generally

dx.doi.org/10.1021/jp400509r | J. Phys. Chem. B 2013, 117, 3917−3926

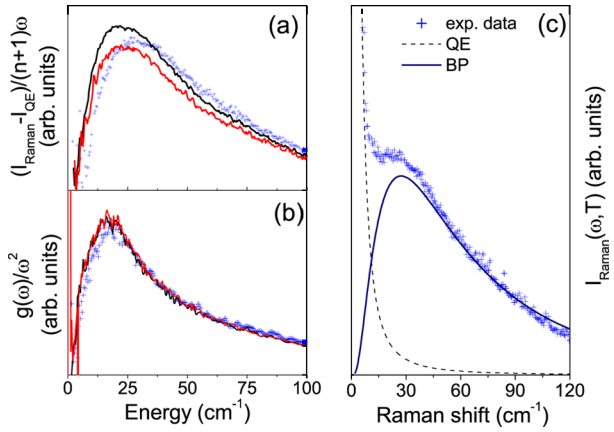

Figure 6. Reduced Raman spectra after subtraction of QE contribution (a) and $g(\omega)/\omega^2$ as obtained by neutron data (b) for pure Met-β-CD (blue +) and inclusion complexes formed by Met-β-CD with (*R*,*S*)-IBP (black line) and (*S*)-IBP (red line) in the energy range 0−100 cm^{-1}. (c) Experimental Raman intensity of Met-β-CD shown together with the different components resulting from the fitting procedure: Lorentz function (dashed line) for the QE contribution and log-normal functional form for the BP (blue continuous line).

observed in the inelastic light and neutron spectra of glassy materials, including polymers[37−39] and cyclodextrin-based polymers,[36] provides a clear indication for the amorphous state of the pure host molecular system.

In the panel of Figure 6c, the two different spectral components of the Met-β-CD Raman profile are highlighted, as resulting from the fitting procedure:[36,38] besides on the Lorentzian function $I_{QE}(\omega)$, used to reproduce the QE contribution (dashed line), a log-normal distribution function having width *W* and amplitude *B* was employed to describe the shape and to take into account the wavenumber position ω_{BP} of the maximum of the Boson peak (continuous line):

$$I_{Raman}(\omega) = I_{QE}(\omega) + B \exp\left\{-\frac{[\ln(\omega/\omega_{BP})]^2}{2W^2}\right\} \quad (9)$$

The data handling procedure described above allows one to estimate the best-fit value for the wavenumber position of the BP for Met-β-CD, which turned out to be ω_{BP} = 27 cm^{-1}.

On the other hand, the quasi-elastic signal isolated by the experimental Raman profile of Met-β-CD appears more intense with respect to the case of pure IBP (see Figure 1), in agreement with QENS results.[25] This occurrence is consistent with the activation, for the host, of additional degrees of freedom over the harmonic behavior, mainly connected to the relaxation of the hydrogen-bonding network formed by the hydroxyl groups of Met-β-CD and the crystallization residual water molecules.

The curves reported in Figure 6a,b point out significant variations in the low-frequency vibrational dynamics of IBP as a consequence of its confinement in the Met-β-CD cavity.

First, we can observe that, after the inclusion inside Met-β-CD cavity, the vibrational behavior of racemic and enantiomeric IBP is the same, and tends to reproduce the one of the macrocycle itself. This experimental finding, together with the absence of rather sharp vibrational peaks in the spectra of IBP inclusion complexes below 200 cm^{-1}, suggests that the complexation process gives rise to a complete amorphization of the pure drug. This is fully consistent with what was already reported in the literature for a variety of inclusion complexes formed by cyclodextrins with different types of guest molecules and with what was observed in previous FTIR-ATR and neutron scattering studies on IBP-complexes.[48−50]

By comparing the spectra reported in Figure 6a,b, a small but significant shift of the wavenumber position of the free BP can be observed with respect to complexed BP. To achieve a more quantitative analysis of the modifications occurring on BP as a consequence of complexation, the same fitting procedure adopted for the Raman spectrum of Met-β-CD (eq 9) was followed for estimating the best-fit values of ω_{BP} for the (*R*,*S*)-IBP and (*S*)-IBP inclusion complexes, which were found, for both of the complexes, to be centered at about 23 cm^{-1}.

It should be pointed out that the trend of the curves obtained after subtraction of the QE contribution and reported in Figure 6a is the same as observed in the raw experimental profiles, thus confirming that the described subtraction procedure of the QE contribution does not affect our final considerations.

The same shift of about 3−4 cm^{-1} toward lower frequencies found for ω_{BP} in Raman spectra is clearly observed also in the corresponding $g(\omega)/\omega^2$ (Figure 6b), which shows the bump moving from about 19 to 16 cm^{-1} as a consequence of complexation.

As is widely reported in literature, the frequency position of BP was found to be sensitive to changes in the elastic properties of disordered systems, over a mesoscopic length scale, as induced by pressure,[37,38] temperature,[51] chemical vetrification,[52] and density.[38,53,54] The experimental results reported in this work give indication that the complexation phenomenon is able to affect the vibrational dynamics of the system over a mesoscopic length scale, by inducing elastic medium modifications, which lead to a general softness of the material.[36]

Further findings on the effect of complexation phenomena on the vibrational dynamics of IBP can be achieved by comparing the dynamic susceptibility $\chi''(\omega)$ as obtained by Raman and INS data for pure Met-β-CD (blue +) and its inclusion complexes formed with (*R*,*S*)-IBP (black line) and (*S*)-IBP (red line) (Figure 7a and b, respectively). This representation of the scattering data allows one to enhance the high frequency part of the density of vibrational states.

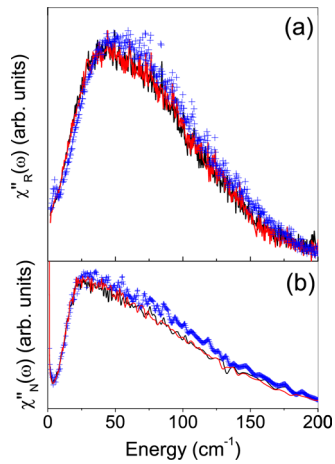

Figure 7. Dynamic susceptibility $\chi''(\omega)$ as obtained by the low-energy Raman (a) and INS (b) spectra for pure Met-β-CD (blue +) and inclusion complexes formed by Met-β-CD with (*R*,*S*)-IBP (black line) and (*S*)-IBP (red line) in the energy range 0−200 cm^{-1}.

dx.doi.org/10.1021/jp400509r | J. Phys. Chem. B 2013, 117, 3917−3926

The comparison between the spectra of free and complexed Met-β-CD shows a change in the shape of vibrational profile for $\omega > \omega_{BP}$ when both (*R*,*S*)- and (*S*)-IBP molecules are entrapped in the CD cavity. This suggests, on one side, a similar complexation mechanism for (*S*)-IBP and (*R*,*S*)-IBP, according to previous results obtained by using FTIR-ATR spectroscopy.[23,24] On the other hand, the different profile of $\chi''(\omega)$ observed for pure host with respect to its inclusion complexes gives evidence of a partial hindering of high-frequency modes of Met-β-CD between 50 and 150 cm^{-1}, as a consequence of the inclusion of IBP in its cavity.

C. The Raman Coupling Function. The Raman coupling function $C^R(\omega)$ measures the efficiency of the coupling between the incident photon and the vibrations of the system, and its frequency dependence plays a relevant role in clarifying the origin of the anomalies in disordered systems.[35,55−57] In particular, an interesting problem is understanding if the $C^R(\omega)$ shows a universal behavior in different kinds of disordered systems. From a theoretical point of view, several models that predict a power-law frequency dependence for $C^R(\omega)$[58−60] have been proposed, but the value of the exponents is still subject of debate: for example, a quadratic dependence[61] $C^R(\omega) \propto \omega^2$ or $C^R(\omega) = cost$[60] has been found in the framework of soft potential model, while in the fracton-like model a power-law $C^R(\omega) \propto \omega^\alpha$ has been estimated.[62,63] In our opinion, the direct comparison between the experimental Raman and neutron scattering data is the most reliable tool to determine the function $C^R(\omega)$.

In Figure 8a−c, we compare the $g(\omega)/\omega^2$ with the corresponding reduced Raman intensity $I^{red}(\omega)$ for pure and complexed Met-β-CD. All of the experimental profiles show the Boson peak centered at about 23−26 cm^{-1} in Raman spectra and at about 16−19 cm^{-1} in the neutron intensities (see, for example, inset of Figure 8a). A strong QE contribution al lower frequencies is found in both Raman and neutron data for all of the examined samples.

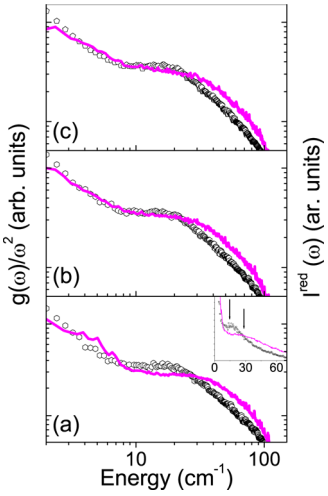

Figure 8. Comparison between the $g(\omega)/\omega^2$ as obtained from neutron data (open symbols) and reduced Raman intensity $I^{red}(\omega)$ (solid line) for pure Met-β-CD (a) and their inclusion complexes formed with (*R*,*S*)-IBP (b) and (*S*)-IBP (c) in the energy range 0−150 cm^{-1}. Inset: Comparison between the position of BP as observed in neutron (open symbols) and Raman spectra (solid line).

By inspection of Figure 8, we note that the Raman and neutron data have the same frequency dependence at low ω for all of the reported profiles, while they differ for $\omega > 50$ cm^{-1}. Moreover, the maxima of ω_{BP} as observed in Raman profiles is found at higher energies with respect to neutron data for both pure host molecule Met-β-CD and its IBP inclusion complexes, as was previously observed in glass forming systems.[55−57]

These findings are reflected in the spectral shape of the Raman coupling function $C^R(\omega)$, which can be estimated according to the approach described in the Theoretical Background.

In Figure 9, we show the behavior of $C^R(\omega)$ for the samples of pure Met-β-CD (blue +) and its inclusion complexes formed with racemic and enantiomeric IBP (black and red lines, respectively) in the energy range 0−150 cm^{-1}. The curves are normalized on their maximum value intensity.

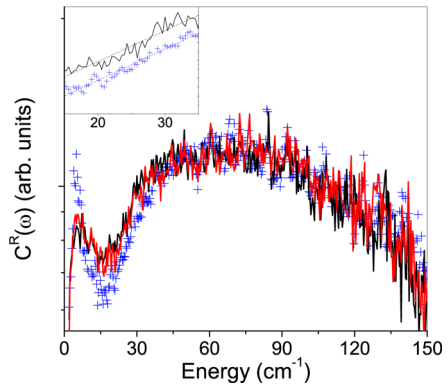

Figure 9. $C^R(\omega)$ calculated combining eqs 1 and 6 for pure Met-β-CD (blue +) and their inclusion complexes formed with (*R*,*S*)-IBP (black line) and (*S*)-IBP (red line) in the energy range 0−150 cm^{-1}. The curves are normalized on their maximum value intensity. Inset: Comparison between $C^R(\omega)$ estimated for Met-β-CD and (*R*,*S*)-IBP inclusion complexes together with the best fit (dashed lines) for $\omega < \omega_{BP}$.

The profiles in Figure 9 turn out to exhibit a similar general behavior for all of the examined samples: (i) for $\omega < 15$ cm^{-1} $C^R(\omega)$ decreases with increasing frequency, (ii) in the energy range of BP, that is, for 20 cm^{-1} < ω < 40 cm^{-1}, $C^R(\omega)$ shows a linear frequency dependence (see inset of Figure 9), (iii) for 50 cm^{-1} < ω < 90 cm^{-1} $C^R(\omega)$ appears to be constant, and, finally, (iv) $C^R(\omega)$ tends to sharply decrease at higher frequencies.

This complex spectral profile observed for $C^R(\omega)$ reflects the different kinds of excitations (localized vibrations, relaxations, high-frequency modes), which contribute to the energy dependence of Raman coupling function in different frequency regimes.

For $\omega < 15$ cm^{-1} the behavior of $C^R(\omega)$ indicates that the Raman spectroscopy is more sensitive to the quasi elastic scattering with respect to the neutron experiments. On the other hand, $C^R(\omega)$ is found to have a linear frequency dependence in the spectral region of BP (20−40 cm^{-1}), thus explaining the shift to higher energies observed in the BP maximum in Raman scattering spectra with respect to neutron data (inset of Figure 8a). The exhibition of a similar linear dependence for $C^R(\omega)$, already observed in other glassy systems,[35,55−57] suggests that this behavior is more common than might be expected.

It is noteworthy that the same slope in the linear increasing of $C^R(\omega)$ is observed for both pure Met-β-CD and its IBP inclusion complexes (inset of Figure 9). This finding gives evidence that the complexation process does not significantly

dx.doi.org/10.1021/jp400509r | J. Phys. Chem. B 2013, 117, 3917−3926

affect the coupling between the probe, that is, light, and the target in the case of both (*S*)-IBP and (*R*,*S*)-IBP and suggests a general behavior of $C^R(\omega)$ in the energy range of BP. On the other hand, the slightly higher intensity of $C^R(\omega)$ observed between 20 and 40 cm^{-1} for inclusion complexes with respect to pure CD reflects the increasing of the QE scattering, observed in the experimental Raman profiles when the IBP molecules are included in the Met-*β*-CD cavity. This occurrence is consistent with the amorphization associated with complexation, as revealed by inelastic light and neutron data, which also contributes to the activation of additional degrees of freedom over the harmonic behavior for inclusion complexes of IBP.

CONCLUSION

The effects on the low-frequency vibrational dynamics of ibuprofen in its racemic and (*S*)-enantiomeric forms as a consequence of complexation in methyl-*β*-cyclodextrin cavity are here explored by Raman and inelastic neutron scattering experiments. Significant differences are observed in the vibrational spectra of free (*R*,*S*)-IBP and (*S*)-IBP in the energy range below 100 cm^{-1}, which have been explained by taking into account their distinct symmetry properties.

The comparison between the low-wavenumber Raman and neutron spectra of pure Met-*β*-CD and its inclusion complexes formed with IBP points out the presence of the so-called Boson peak, strongly supporting the complete amorphization of the drug as a consequence of its inclusion in the CD cavity. Moreover, a shift to lower energies of the maximum of BP and a partial hindering of high-frequency modes of pure host Met-*β*-CD between 50 and 150 cm^{-1} are observed when IBP is confined in CD cavity. These findings suggest that the complexation phenomenon is able to significantly affect the vibrational dynamics of the system over the frequency range below 200 cm^{-1}.

Finally, the comparison between Raman and INS data allows one to estimate the light-to-excitation coupling function $C^R(\omega)$, providing important information on the nature of the vibrational modes in the inclusion complexes.

The overall results add significant new information to achieve an exhaustive picture of the "host−guest" interactions involved in the complexation phenomena of cyclodextrins, retaining a prerequisite for improving their application as carriers and their role in the development of innovative drug delivery systems.

ASSOCIATED CONTENT

Supporting Information

Full list of atom labeling for the structures of (*R*,*S*)-IBP and (*S*)-IBP. This material is available free of charge via the Internet at http://pubs.acs.org.

AUTHOR INFORMATION

Corresponding Author

*Phone: +39 0461 282940. E-mail: rossi@science.unitn.it.

Notes

The authors declare no competing financial interest.

ACKNOWLEDGMENTS

We thank Dr. Marco Zanatta for useful discussions. B.R. acknowledges financial support from the Regione Veneto, being the beneficiary of a scholarship within the Programma Operativo Regionale FSE 2007-2013.

REFERENCES

(1) Schneider, H.; Yatsimirsky, A. *Principle and Methods in Supramolecular Chemistry*; Wiley: New York, 2000.
(2) Whitesides, G. M.; Grzybowski, B. A. Self-Assembly at All Scales. *Science* **2002**, *295*, 2418−2421.
(3) Li, S.; Purdy, W. C. Cyclodextrins and their Applications in Analytical Chemistry. *Chem. Rev.* **1992**, *92*, 1457−1470.
(4) Szejtli, J. Introduction and General Overview of Cyclodextrin Chemistry. *Chem. Rev.* **1998**, *98*, 1743−1754.
(5) Uekama, K.; Hirayama, F.; Irie, T. Cyclodextrin Drug Carrier Systems. *Chem. Rev.* **1998**, *98*, 2045−2076.
(6) Bender, M. L.; Komiyama, M. *Cyclodextrin Chemistry*; Springer-Varlag: New York, 1978.
(7) Szejtli, J. *Cyclodextrin Technology*; Kluwer Academic Publishers: Boston, 1988.
(8) Szejtli, J.; Osa, T. *Comprehensive Supramolecular Chemistry (CDs)*; Pergamon: Oxford, 1996.
(9) Harata, K. Structural Aspects of Stereodifferentiation in the Solid State. *Chem. Rev.* **1998**, *98*, 1803−1827.
(10) Amajjahe, S.; Choi, S.; Muntenau, M.; Ritter, H. Pseudopolyanions Based on Poly(NIPAAM-co-*β*-Cyclodextrin Methacrylate) and Ionic Liquids. *Angew. Chem., Int. Ed.* **2008**, *47*, 3435−3437.
(11) Takashima, T.; Osaki, M.; Harada, A. Cyclodextrin-Initiated Polymerization of Cyclic Esters in Bulk: Formation of Polyester-Tethered Cyclodextrins. *J. Am. Chem. Soc.* **2004**, *126*, 13588−13589.
(12) Uekama, K.; Irie, T. *Cyclodextrins and Their Industrial Uses*; De Santé: Paris, 1987.
(13) Núñez-Agüero, C. J.; Escobar-Llanos, C. M.; Díaz, D.; Jaime, C.; Garduño-Juárez, R. Chiral Discrimination of Ibuprofen Isomers in *β*-cyclodextrin Inclusion Complexes: Experimental (NMR) and Theoretical (MD, MM/GBSA) Studies. *Tetrahedron* **2006**, *62*, 4162−4172.
(14) Tazerouti, F.; Badjah-Hadj-Ahmed, A. Y.; Meklati, B. Y.; Franco, P.; Minguillon, C. Enantiomeric Separation of Drugs and Herbicides on a *β*-cyclodextrin-bonded Stationary Phase. *Chirality* **2002**, *14*, 59−66.
(15) Salvatierra, D.; Sánchez-Ruiz, X.; Garduño-Juárez, R.; Cervelló, E.; Jaime, C.; Virgili, A.; Sánchez-Fernando, F. Enantiodifferentiation by Complexation with *β*-Cyclodextrin: Experimental (NMR) and Theoretical (MD, FEP) Studies. *Tetrahedron* **2000**, *56*, 3035−3041.
(16) Wenz, G.; Han, B. H.; Müller, A. Cyclodextrin Rotaxanes and Polyrotaxanes. *Chem. Rev.* **2006**, *106*, 782−817.
(17) Wenz, G. Recognition of Monomers and Polymers by Cyclodextrins. *Adv. Polym. Sci.* **2009**, *222*, 1−54.
(18) Alexander, J. M.; Clark, J. L.; Brett, T. J.; Stezowski, J. J. Chiral Discrimination in Cyclodextrin Complexes of Amino Acid Derivatives: *β*-cyclodextrin/N-acetyl-L-phenylalanine and N-acetyl-D-phenylalanine Complexes. *Proc. Natl. Acad. Sci. U.S.A.* **2002**, *99*, 5115−5120.
(19) Barbato, F.; La-Rotonda, M.; Quaglia, F. Interactions of Nonsteroidal Antiinflammatory Drugs with Phospholipids: Comparison between Octanol/buffer Partition Coefficients and Chromatographic Indexes on Immobilized Artificial Membranes. *J. Pharm. Sci.* **1997**, *86*, 225−229.
(20) Su, X. Y.; Al-Kassas, R.; Li Wan, P. A. Statistical Modelling of Ibuprofen Release from Spherical Lipophilic Matrices. *Eur. J. Pharm. Biopharm.* **1994**, *40*, 73−76.
(21) Rossi, B.; Verrocchio, P.; Viliani, G.; Mancini, I.; Guella, G.; Rigo, E.; Scarduelli, G.; Mariotto, G. Vibrational Properties of Ibuprofen−Cyclodextrin Inclusion Complexes Investigated by Raman Scattering and Numerical Simulation. *J. Raman Spectrosc.* **2009**, *40*, 453−458.
(22) Crupi, V.; Guella, G.; Majolino, D.; Mancini, I.; Rossi, B.; Stancanelli, R.; Venuti, V.; Verrocchio, P.; Viliani, G. T-Dependence of the Vibrational Dynamics of IBP/diME-*β*-CD in Solid State: A FT-IR Spectral and Quantum Chemical Study. *J. Mol. Struct.* **2010**, *972*, 75−80.
(23) Crupi, V.; Majolino, D.; Venuti, V.; Guella, G.; Mancini, I.; Rossi, B.; Verrocchio, P.; Viliani, G.; Stancanelli, R. Temperature Effect on the Vibrational Dynamics of Cyclodextrin Inclusion Complexes:

Investigation by FTIR-ATR Spectroscopy and Numerical Simulation. *J. Phys. Chem. A* **2010**, *114*, 6811−6817.
(24) Crupi, V.; Guella, G.; Majolino, D.; Mancini, I.; Paciaroni, A.; Rossi, B.; Venuti, V.; Verrocchio, P.; Viliani, G. Effect of the Chiral Discrimination on the Vibrational Properties of (R)-, (S)- and (R,S)-Ibuprofen/methyl-β-cyclodextrin Inclusion Complexes. *Philos. Mag.* **2011**, *91*, 1776−1785.
(25) Crupi, V.; Guella, G.; Longeville, S.; Majolino, D.; Mancini, I.; Paciaroni, A.; Rossi, B.; Venuti, V., submitted.
(26) Crupi, V.; Guella, G.; Majolino, D.; Mancini, I.; Rossi, B.; Stancanelli, R.; Venuti, V.; Verrocchio, P.; Viliani, G. A Phase Solubility Study on the Chiral Discrimination of Ibuprofen by β-Cyclodextrin Complexes. *Food Biophys.* **2011**, *6*, 267−273.
(27) Hedoux, A.; Decroix, A.; Guinet, Y.; Paccou, L.; Derollez, P.; Descamps, M. Low- and High-Frequency Raman Investigations on Caffeine: Polymorphism, Disorder and Phase Transformation. *J. Phys. Chem. B* **2011**, *115*, 5746−5753.
(28) Evrard, B.; Bertholet, P.; Gueders, M.; Flament, M.-P.; Piel, G.; Gayot, A.; Leterme, P.; Foidart, J.-M.; Cataldo, D. Cyclodextrins as a Potential Carrier in Drug Nebulization. *J. Controlled Release* **2004**, *96*, 403−410.
(29) Cavalli, R.; Peira, E.; Caputo, O.; Gasco, M. R. Solid Lipid Nanoparticles as Carriers of Hydrocortisone and Progesterone Complexes with β-cyclodextrins. *Int. J. Pharm.* **1999**, *182*, 59−69.
(30) Frisch, M. J.; Trucks, G. W.; Schlegel, H. B.; Scuseria, G. E.; Robb, M. A.; Cheeseman, J. R.; Montgomery, J. A., Jr.; Vreven, T.; Kudin, K. N.; Burant, J. C.; et al. *Gaussian 03*, revision C.02; Gaussian, Inc.: Wallingford, CT, 2004.
(31) Shuker, R.; Gammon, R. W. Raman-Scattering Selection-Rule Breaking and the Density of States in Amorphous Materials. *Phys. Rev. Lett.* **1970**, *25*, 222−225.
(32) Galenneer, F. L.; Sen, P. L. Theory for the First-Order Vibrational Spectra of Disordered Solids. *Phys. Rev. B* **1978**, *17*, 1928−1933.
(33) Carini, G.; D'Angelo, G.; Tripodo, G.; Fontana, A.; Leonardi, A.; Saunders, G. A.; Brodin, A. Excess of Low-Energy Excitations in Glasses. *Phys. Rev. B* **1995**, *52*, 9342−9353.
(34) Majolino, D.; Mallamace, F.; Migliardo, P.; Aliotta, F.; Micali, N.; Vasi, C. Spectral Evidence of Connected Structures in Liquid Water: Effective Raman Density of Vibrational States. *Phys. Rev. E* **1993**, *47*, 2669−2675.
(35) Fontana, A.; Dell'Anna, R.; Montagna, M.; Rossi, F.; Viliani, G.; Ruocco, G.; Sampoli, M.; Buchenau, U.; Wischnewski, A. The Raman Coupling Function in Amorphous Silica and the Nature of the Long-Wavelength Excitations in Disordered Systems. *Europhys. Lett.* **1999**, *47*, 56−62.
(36) Rossi, B.; Caponi, S.; Castiglione, F.; Corezzi, S.; Fontana, A.; Giarola, M.; Mariotto, G.; Mele, A.; Petrillo, C.; Trotta, F.; et al. Networking Properties of Cyclodextrin-Based Cross-Linked Polymers Probed by Inelastic Light-Scattering Experiments. *J. Phys. Chem. B* **2012**, *116*, 5323−5327.
(37) Niss, K.; Begen, B.; Frick, B.; Ollivier, J.; Beraud, A.; Sokolov, A.; Novikov, V. N.; Alba-Simionesco, C. Influence of Pressure on the Boson Peak: Stronger than Elastic Medium Transformation. *Phys. Rev. Lett.* **2007**, *99*, 1−4.
(38) Hong, L.; Begen, B.; Kisliuk, A.; Alba-Simionesco, C.; Novikov, V. N.; Sokolov, A. P. Pressure and Density Dependence of the Boson Peak in Polymers. *Phys. Rev. B* **2008**, *78*, 1−11.
(39) Hong, L.; Gujrati, P. D.; Novikov, V. N.; Sokolov, A. P. Molecular Cooperativity in the Dynamics of Glass-forming Systems: A New Insight. *J. Chem. Phys.* **2009**, *131*, 1−7.
(40) Freer, A. A.; Bunyan, J. M.; Shankland, N.; Sheen, D. B. Structure of (s)-(+)-ibuprofen. *Acta Crystallogr.* **1993**, *C49*, 1378−1380.
(41) Perlovich, G. L.; Kurkov, S. V.; Hansen, L. K. R.; Bauer-Brand, A. Thermodynamics of Sublimation, Crystal Lattice Energies and Crystal Structures of Racemates and Enantiomers:(+)- and (-)-ibuprofen. *J. Pharm. Sci.* **2004**, *93*, 654−666.
(42) Bogdanova, S.; Pareva, I.; Nikolova, P.; Tskavoska, I.; Muller, B. Interactions of Poly(vinylpyrrolidone) with Ibuprofen and Naproxen: Experimental and Modeling Studies. *Pharm. Res.* **2005**, *22*, 806−815.
(43) Benassi, P.; Fontana, A.; Frizzera, W.; Montagna, M.; Mazzacurati, V.; Signorelli, G. Disorder-induced Light Scattering in Solids: The Origin of the Boson Peak in Glasses. *Philos. Mag. B* **1995**, *71*, 761−769.
(44) Sokolov, A. P.; Kisliuk, A.; Quitmann, D.; Duval, E. Evaluation of Density of Vibrational States of Glasses from Low-frequency Raman Spectra. *Phys. Rev. B* **1993**, *48*, 7692−7695.
(45) Buchenau, U.; Wischnewski, A.; Ohl, M.; Fabiani, E. Neutron Scattering Evidence on the Nature of the Boson Peak. *J. Phys.: Condens. Matter* **2007**, *19*, 1−15.
(46) Fontana, A.; Rossi, F.; Carini, G.; D'Angelo, G.; Tripodo, G.; Bartolotta, A. Low-Energy Vibration Excess in Silica Xerogels. *Phys. Rev. Lett.* **1997**, *78*, 1078−1081.
(47) Fabiani, E.; Fontana, A.; Buchenau, U. Neutron Scattering Study of the Vibrations in Vitreous Silica and Germania. *J. Chem. Phys.* **2008**, *128*, 1−12.
(48) Hladoń, T.; Pawlaczyk, J.; Szafran, B. Stability of Ibuprofen in its Inclusion Complex with β-cyclodextrin. *J. Inclusion Phenom. Macrocycl. Chem.* **2000**, *36*, 1−8.
(49) Tozuka, Y.; Fujito, T.; Moribe, K.; Yamamoto, K. Ibuprofen-Cyclodextrin Inclusion Complex Formation using Supercritical Carbon Dioxide. *J. Inclusion Phenom. Macrocycl. Chem.* **2006**, *56*, 33−37.
(50) Hussein, K.; Türk, M.; Wahl, M. A. Comparative Evaluation of Ibuprofen/β-cyclodextrin Complexes Obtained by Supercritical Carbon Dioxide and Other Conventional Methods. *Pharm. Res.* **2007**, *24*, 585−592.
(51) Caponi, S.; Fontana, A.; Rossi, F.; Baldi, G.; Fabiani, E. Effect of Temperature on the Vibrational Density of States in Vitreous SiO2: A Raman Study. *Phys. Rev. B* **2007**, *76*, 1−4.
(52) Caponi, S.; Corezzi, S.; Fioretto, D.; Fontana, A.; Monaco, G.; Rossi, F. Raman-Scattering Measurements of the Vibrational Density of States of a Reactive Mixture During Polymerization: Effect on the Boson Peak. *Phys. Rev. Lett.* **2009**, *102*, 1−4.
(53) Zanatta, M.; Baldi, G.; Caponi, S.; Fontana, A.; Gilioli, E.; Krish, M.; Masciovecchio, C.; Monaco, G.; Orsingher, L.; Rossi, F.; et al. Elastic Properties of Permanently Densified Silica: A Raman, Brillouin Light, and X-ray Scattering Study. *Phys. Rev. B* **2010**, *81*, 1−4.
(54) Pilla, O.; Angelani, L.; Fontana, A.; Goncalves, J. R.; Ruocco, G. Structural and Dynamical Consequences of Density Variation in Vitreous Silica. *J. Phys.: Condens. Matter* **2003**, *15*, S995−S1005.
(55) Fontana, A.; Rossi, F.; Viliani, G.; Ruocco, G.; Dal Maschio, R. The Raman Coupling Function in Disordered Solids: a Light and Neutron Scattering Study on Glasses of Different Fragility. *J. Phys.: Condens. Matter* **2007**, *19*, 1−6.
(56) Fontana, A.; Rossi, F.; Fabiani, E. The Raman Coupling Function in v-GeO2 and v-SiO2: A New Light and Neutron Scattering Study. *J. Non-Cryst. Solids* **2006**, *352*, 4601−4605.
(57) Ivanda, M.; Kiefer, W.; Mariotto, G. Raman Light-to-Vibration Coupling Coefficient of v-SiO2 in Spectral Interval Range up to 600 cm^{-1}. *Solid State Commun.* **2001**, *117*, 423−428.
(58) Stoll, E.; Kolb, M.; Courtens, E. Numerical Verification of Scaling for Scattering from Fractons. *Phys. Rev. Lett.* **1992**, *68*, 2472−2475.
(59) Alexander, S.; Courtens, E.; Vacher, R. Vibrations of Fractals: Dynamic Scaling, Correlation Functions and Inelastic Light Scattering. *Physica A* **1993**, *195*, 286−318.
(60) Gurevich, V. L.; Parshin, D. A.; Pelous, J.; Schober, H. R. Theory of Low-energy Raman Scattering in Glasses. *Phys. Rev. B* **1993**, *48*, 16318−16331.
(61) Martin, A. J.; Brenig, W. Model for Brillouin Scattering in Amorphous Solids. *Phys. Status Solidi B* **1974**, *64*, 163−172.
(62) Fontana, A.; Rocca, F.; Fontana, M. P. Direct Experimental Determination of the Crossover Frequency between Phonon and Fracton Regimes and its Scaling Behavior in Superionic Silver Borate Glasses. *Phys. Rev. Lett.* **1987**, *58*, 503−506.

(63) Fontana, A.; Rocca, F.; Fontana, M. P. Evidence of Fractal Behaviour. *Philos. Mag. B* **1987**, *56*, 251−255.